

Supporting information for:

Enhancing Doping Efficiency by Improving

Host-Dopant Miscibility for Fullerene-Based

n-Type Thermoelectrics

Li Qiu,^{†,‡} Jian Liu,[†] Riccardo Alessandri,^{†,¶} Xinkai Qiu,^{†,‡} Marten Koopmans,[†]
Remco W. A. Havenith,^{†,‡,§} Siewert J. Marrink,^{†,¶} Ryan C. Chiechi,^{†,‡} L. Jan
Anton Koster,^{*,†} and Jan C. Hummelen^{*,†,‡}

[†]*Zernike Institute for Advanced Materials, University of Groningen, Nijenborgh 4, 9747
AG Groningen, The Netherlands*

[‡]*Stratingh Institute for Chemistry, University of Groningen, Nijenborgh 4, 9747 AG
Groningen, The Netherlands*

[¶]*Groningen Biomolecular Sciences and Biotechnology Institute, University of Groningen,
Nijenborgh 7, 9747 AG Groningen, The Netherlands*

[§]*Ghent Quantum Chemistry Group, Department of Inorganic and Physical Chemistry,
Ghent University, Krijgslaan 281 (S3), B-9000 Gent, Belgium*

E-mail: l.j.a.koster@rug.nl; j.c.hummelen@rug.nl

⁰Li Qiu and Jian Liu contributed equally to this work.

Contents

1	Experimental details	S2
1.1	General	S2
1.2	Synthesis	S3
2	Characterization	S3
2.1	Calculated mobility	S3
2.2	Cyclic voltammetry measurements	S6
2.3	AFM measurements	S6
3	Computational details	S8
3.1	Electronic structure calculations	S8
3.2	Coarse-grain molecular dynamics simulations	S8
3.2.1	Force field details	S8
3.2.2	Analysis details	S18
4	NMR spectra	S19
	References	S22

1 Experimental details

1.1 General

General: Analytical TLC was performed on Merck silica gel 60/kieselguhr F254 and visualization was accomplished by UV light. Column chromatography was performed using silica gel (SiliaFlash P60 Type R12030B, 230-400 mesh). ^1H -NMR and ^{13}C -NMR were performed on a Varian Unity Plus (400 MHz) instrument at 25°C , using tetramethylsilane (TMS) as an internal standard. NMR shifts are reported in ppm, relative to the residual protonated

solvent signals of CDCl_3 ($= 7.26$ ppm) or at the carbon absorption in CDCl_3 ($= 77.0$ ppm), and multiplicities are denoted as: s = singlet, d = doublet, t = triplet and m = multiplet. IR measurements were performed on a Nicolet iS50 FT-IR spectrometer. UV-vis absorption spectra were measured with a Jenway 6715 spectrophotometer. High Resolution Mass Spectroscopy (HRMS) was performed on a JEOL JMS 600 spectrometer.

1.2 Synthesis

TEG-DMBI. To the solution of substituted N,N'-dimethyl-o-phenylenediamine (120 mg, 0.88 mmol) in 1 ml of methanol was added 4-(2-(2-(2-ethoxyethoxy)ethoxy)ethoxy)benzaldehyde (280 mg, 0.99 mol) with vigorously shaking at 0°C , then a drop of glacial acetic acid was added.^{S1} The mixture was allowed to warm to room temperature for 2.5 h, then evaporated to give the crude product which was then purified by column chromatography (Neutral Al_2O_3 , Hexane : DCM= 1:1) to give 200 mg desired product as a white solid (57%).

$^1\text{H-NMR}$ (400 MHz, CD_3OD) δ 7.48 (d, $J = 8.6$ Hz, 2H), 6.99 (d, $J = 8.6$ Hz, 2H), 6.65 (dd, $J = 5.4, 3.2$ Hz, 2H), 6.42 (dd, $J = 5.4, 3.2$ Hz, 2H), 4.67 (s, 1H), 4.18 4.13 (m, 2H), 3.89 3.82 (m, 2H), 3.71-3.50 (m, 10H), 2.49 (s, 6H), 1.17 (t, $J = 7.0$ Hz, 3H). $^{13}\text{C-NMR}$ (75 MHz, CD_3OD) δ 162.5, 144.8, 133.5, 132.4, 121.8), 116.8, 108.4, 96.6, 73.0, 72.8, 72.1, 72.0, 69.9, 68.8, 34.9, 16.7. IR (cm^{-1}): 2866, 1719, 1606, 1491, 1452, 1367, 1295, 1243, 1112, 728. HRMS(ESI) calcd. for $\text{C}_{23}\text{H}_{33}\text{N}_2\text{O}_4[\text{M}+\text{H}]^+$: 401.24348, found: 401.24184.

2 Characterization

2.1 Calculated mobility

The estimation of charge carrier density and mobility: According to extended Gaussian disorder model (EGDM),^{S2} the charge carriers in disordered organic semiconductors hop over

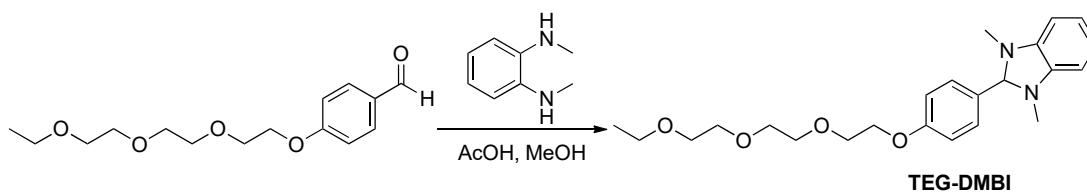


Figure S1: Synthetic route of dopant.

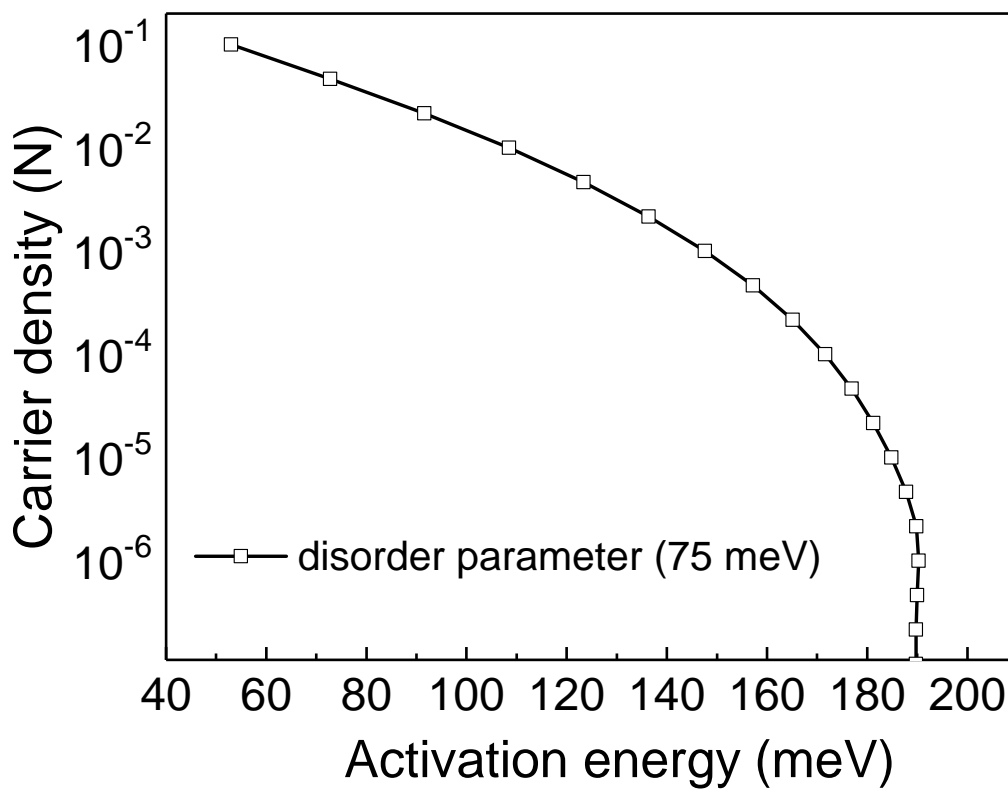


Figure S2: Simulated dependence of the activation energy versus the charge carrier density at an energetic disorder of 75 meV at a temperature range of 260-300 K. N represents the total density of states (10^{21} cm^{-3}).

an energy landscape with a Gaussian density of states (DOS), which is considered a thermally activated process. The charge hopping mobility largely depends on the temperature and on the carrier density. In our previous study,^{S3} we managed to develop a relationship between the activation energy and charge carrier density based on EGDM. Figure S2 shows this activation energy-carrier density-relationship in doped PTEG-1 system with a disorder parameter of 75 meV. The carrier densities were estimated by simply adapting the corresponding activation energy values (in Figure 3A) of differently doped films to the relationship in Figure S2 and are displayed in Figure 3B. As the direct measurement of the mobility in doped PTEG-1 layers is impossible by traditional field-effect transistors, we estimated the mobility values by simply using the formula: ($\mu = \sigma / (ne)$), where μ , e and n are the mobility, elemental charge and charge carrier density, respectively. The n values are from Figure 2B.

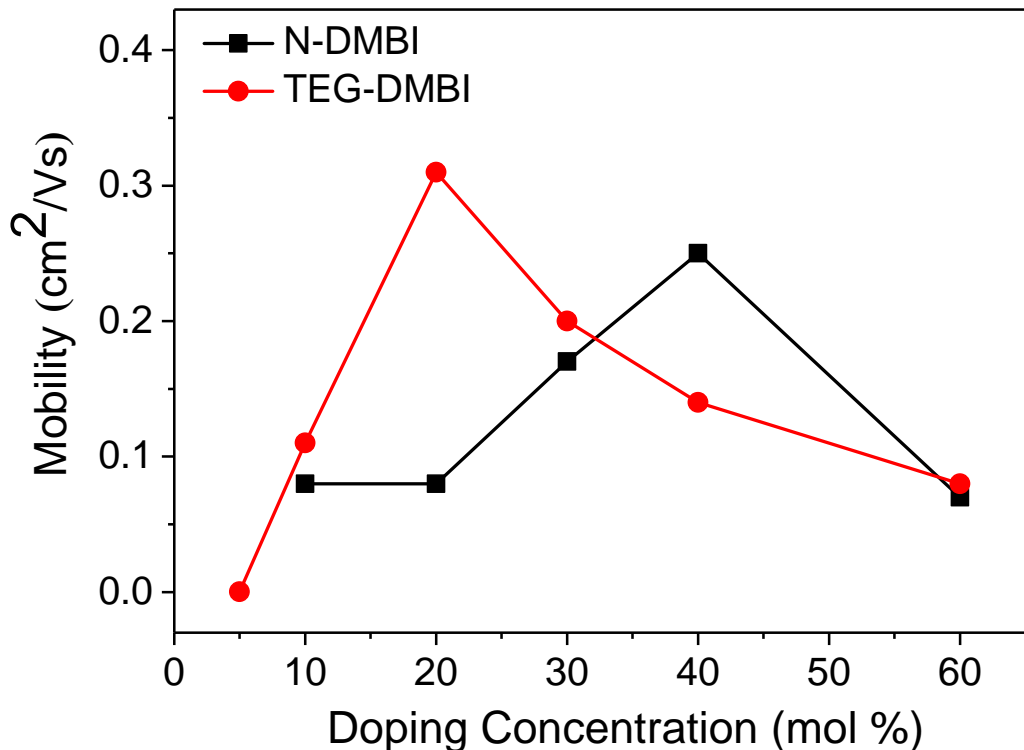


Figure S3: The calculated mobility ($\mu = \sigma / (ne)$) as a function of doping concentration in N-DMBI (black square) and TEG-DMBI (red dot) doped PTEG-1 systems.

2.2 Cyclic voltammetry measurements

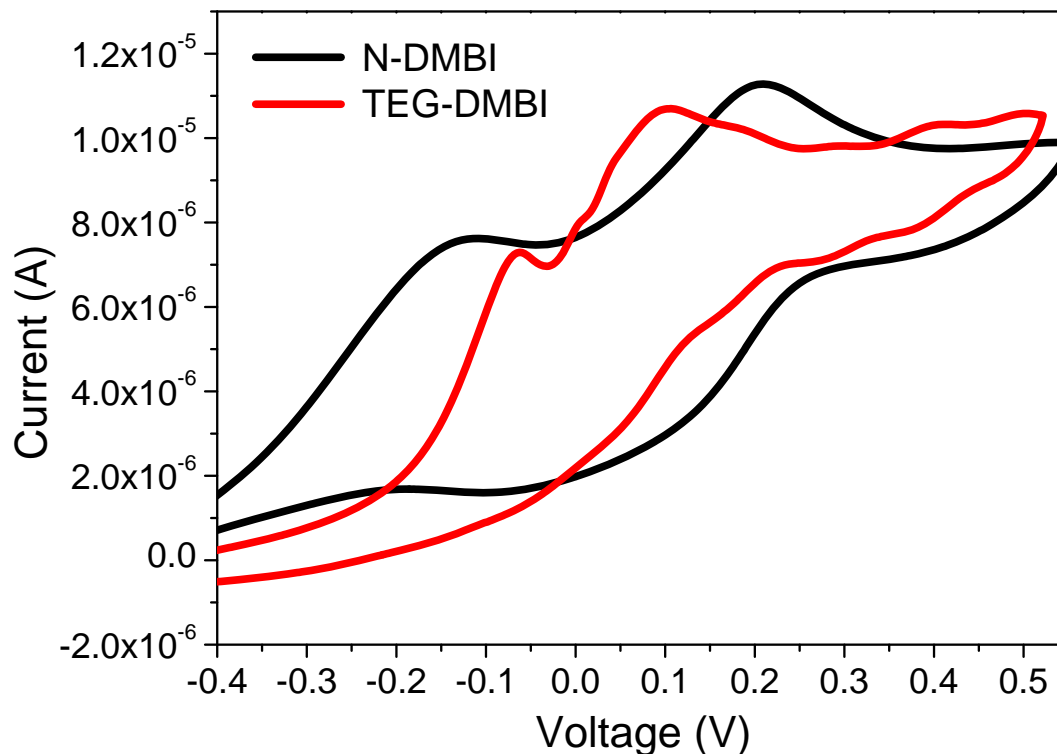


Figure S4: Cyclic voltammetry curves of TEG-DMBI and N-DMBI in deaerated acetonitrile containing 0.1 M $n\text{-Bu}_4\text{NPF}_6$ as supporting electrolyte.

2.3 AFM measurements

We studied the morphology and the phase of the samples by Tapping mode AFM (Bruker, model MMAFM-2). We used RTESPA-300 tips (Bruker, resonant frequency 300 kHz, spring constant 40 N/m, tip radius 8 nm) specifically for the measurements. We scanned all samples at a fixed scan rate of 0.8 Hz and 512 samples/line at a fix aspect ratio of 1. Both height and phase images were processed and analyzed in Nanoscope Analysis provided by Bruker to calculate roughness.

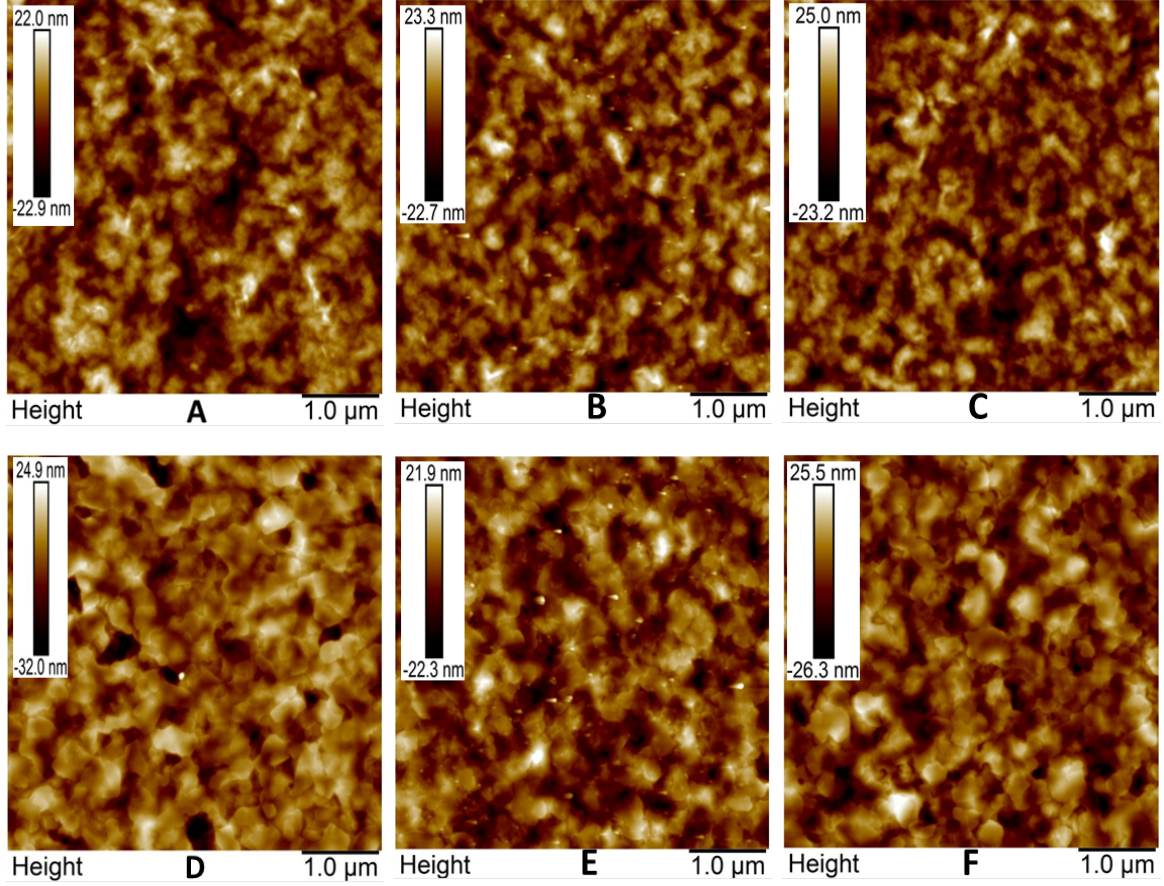


Figure S5: AFM height profiles of PTEG-1 films before (up) and after (below) annealing at 120°C for 1.5 h without (A,D) and with 30 mol% dopants (N-DMBI (B,E), TEG-DMBI (C,F)).

Table S1: Summary of Root-Mean-Square deviation (RMS) and arithmetic average for AFM height images of (un)doped PTEG-1 films.

		undoped	N-DMBI-doped	TEG-DMBI-doped
Before annealing	RMS (nm)	6.48	6.66	7.02
	Ra (nm)	5.21	5.35	5.60
After annealing	RMS (nm)	7.53	6.04	7.38
	Ra (nm)	5.74	4.73	5.89

Table S2: Summary of Root-Mean-Square deviation (RMS) and arithmetic average for AFM phase images of (un)doped PTEG-1 films.

		undoped	N-DMBI-doped	TEG-DMBI-doped
Before annealing	RMS	1.04°	1.90°	1.46°
	Ra	0.81°	1.53°	1.18°
After annealing	RMS	2.28°	1.38°	1.45°
	Ra	1.68°	1.05°	1.08°

3 Computational details

3.1 Electronic structure calculations

SOMO energies. Geometries for both compounds, N-DMBI and TEG-DMBI, were optimized at the B3LYP/6-31G* level of density functional theory (DFT). The imidazole core hydrogen was subsequently removed, and the neutral radical structures were optimized with unrestricted DFT calculations employing two different DFT functionals and the 6-31G* and 6-311G* basis sets. From these calculations, the singly-occupied molecular orbital (SOMO) energies were obtained and are collected in Table S3. The B3LYP/6-31G* SOMO energy agrees well with the energy value of -2.36 eV previously reported for N-DMBI^{S4} and mentioned in the main manuscript. The values with different functionals and bigger basis sets only shift the SOMO energy of both dopants, not changing their difference ($|\Delta E|$), which remains virtually the same in all cases (about 0.2 eV). The B3LYP/6-311G* optimized structures of both dopants are available for download as part of the Supporting Information.

Table S3: SOMO energies (in eV) at different levels of theory.

	B3LYP/6-31G*	B3LYP/6-311G*	PBE/6-31G*	PBE/6-311G*
N-DMBI	-2.35	-2.59	-1.78	-2.02
TEG-DMBI	-2.56	-2.79	-1.98	-2.22
$ \Delta E $	0.21	0.20	0.20	0.20

3.2 Coarse-grain molecular dynamics simulations

3.2.1 Force field details

PTEG-1. A PTEG-1 Martini^{S5} CG model has been built by merging the available triethylene glycol (TEG) model^{S6-S8} (see below) to a newly developed model for the 2-Phenyl-N-methyl-Pyrrolidino[[3',4':1,2]][C60]fullerene (PP) moiety. The latter, a functionalized fullerene,

has been built following the procedure described in our recent work for the PCBM fullerene derivative^{S9} and details are described below.

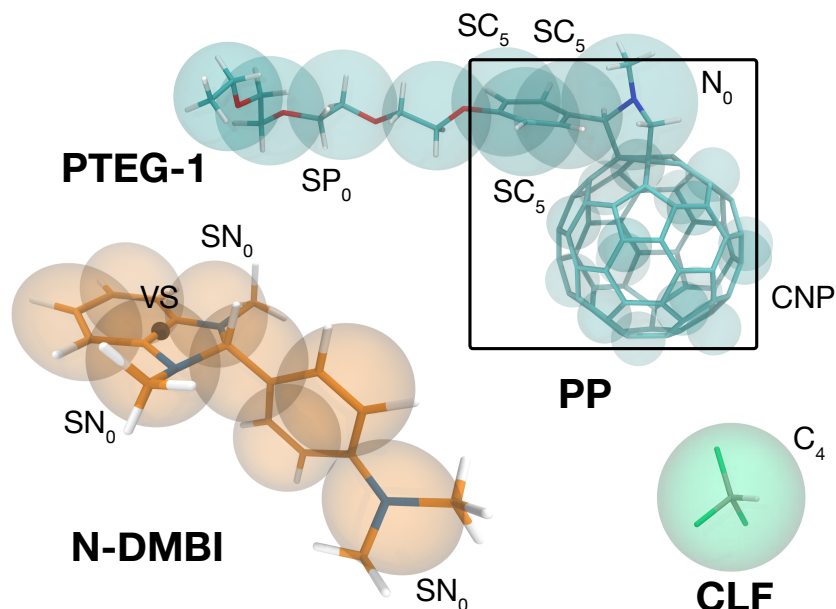


Figure S6: CG site positions (and types) and underlying atomistic structures for the molecules involved in the present study. The radius of the CG interaction sites is not represented in scale (*e.g.*, the beads describing C60 are depicted with a smaller radius) for clarity. In the case of N-DMBI, where not indicated, the CG particle type is SC5.

The Martini 16-beads model, developed by Monticelli,^{S10} is used for the description of C₆₀ fullerene. The N-methyl-pyrrolidine moiety is represented by a N0 bead, while the phenyl substituent in position 2 of the pyrrolidine by three SC5 particles, following the standard model for benzene. A representation of the atomistic structure underlying the CG particles is shown in Figure S6. The ethylene glycol units are described as SP0 particles, following the model of poly ethylene glycol/oxide (PEG/PEO) developed by Rossi and co-workers.^{S7}

All the bonded parameters for the PTEG-1 CG model (excluded the ones involving exclusively F16 beads, for which we refer to Ref. S10) are collected in Table S4. The dihedral ϕ_1 is necessary to reproduce the atomistic distribution of the dihedral angle around the bond connecting the pyrrolidine and phenyl moieties, dihedral which has been checked by quantum mechanical (QM) calculations (see **Atomistic models** section). The (improper) dihedrals ϕ_2 and ϕ_3 are added to keep the side chain orientation fixed with respect to the

Table S4: PTEG-1 CG bonded parameters (bonds, $b_1 - b_6$, angles $\theta_1 - \theta_4$, dihedrals $\phi_1 - \phi_5$).

Bead types (labels)		b_0 (nm)	κ_b (kJ mol ⁻¹ nm ⁻²)	
b_1	CNP-N0 (C08-N17)	0.220	constraint	
b_2	CNP-SC5 (C08-C18)	0.295	5000	
b_3	N0-SC5 (N17-C18)	0.255	constraint	
b_4	SC5-SC5 (C18-C19, C18-C20, C19-C20)	0.270	constraint	
b_5	SC5-SP0 (C19-P21, C20-P21)	0.325	10000	
b_6	SP0-SP0 (P21-P22, P22-P23, P23-P24)	0.330	17000	
		θ_0 (deg)	κ_θ (kJ mol ⁻¹)	
θ_1	CNP-CNP-N0 (C09-C08-N17)	109	350 ^a	
θ_2	CNP-N0-SC5 (C08-N17-C18)	80	350 ^a	
θ_3	N0-SC5-SC5 (N17-C18-C19)	120	200 ^a	
θ_4	SC5-SC5-SP0 (C18-C19,C20-P21)	122	50	
θ_5	SP0-SP0-SP0 (P21-P22-P23, P22-P23-P24)	130	25 ^a	
		130	50	
		ϕ_0 (deg)	κ_ϕ (kJ mol ⁻¹ rad ⁻²)	n
ϕ_1	CNP-N0-SC5-SC5 (C08-N17-C19-C18)	65.00	40.00	2
ϕ_2	CNP-SC5-N0-CNP (C09-C18-N17-C08)	15.00	100.00	
ϕ_3	CNP-N0-SC5-CNP (C09-N17-C18-C03)	-25.00	100.00	
ϕ_4	N0-SC5-SC5-SC5 (N17-C19-C20-C18)	14.00	350.00	
ϕ_5	SP0-SP0-SP0-SP0 (P21-P22-P23-P24)	180.00	1.96	1
		0.00	0.18	2
		0.00	0.33	3
		0.00	0.12	4

^a Resticted Bending Potential (function type 10 in GROMACS 5.x).

beads describing C_{60} according to PP atomistic structure. Bonded parameters for the TEG model make use of the Restricted Bending Potential (ReB) as proposed in Ref. S8. This allows for improved numerical stability.^{S8} Such potential forms were found necessary also for other angles (θ_1 , θ_2 , and θ_3) involving exclusively PP beads. Comparison between bond and angle distributions obtained at the atomistic and CG levels are shown in Figure S7.

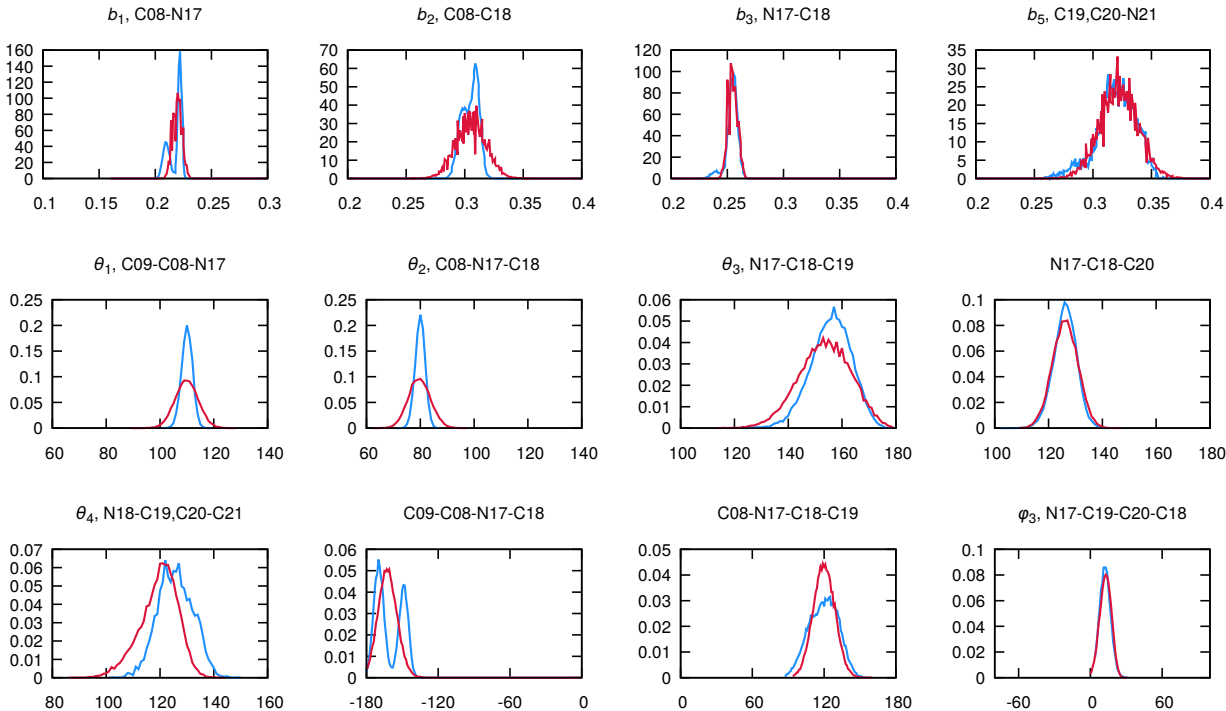


Figure S7: Bond and angle distributions for PTEG-1 (Martini in red, GROMOS in blue). Each header indicates the degree of freedom whose distribution is shown (compare to Table S4).

Dopants. Martini models for the two dopant molecules, N-DMBI and TEG-DMBI, have been developed. SC5 beads are used to describe the phenyl-benzimidazole backbone, with SN0 particles used for groups of atoms containing nitrogen atoms. A schematic representation of N-DMBI atomistic structure and its CG mapping is shown in Figure S6. For the TEG-derivative, the SN0 bead representing the dimethylamino group is replaced by four SP0 beads describing a TEG chain, as done for the PTEG-1 model. All the bonded parameters for N-DMBI are shown in Table S5, while the parameters for the TEG side chain of TEG-

DMBI are the same that are used for PTEG-1, thus we refer to Table S4. The (improper)

Table S5: N-DMBI CG bonded parameters (bonds $b_1 - b_5$, dihedrals $\phi_1 - \phi_3$).

	Bead types (labels)	b_0 (nm)	κ_b (kJ mol ⁻¹ nm ⁻²)	
b_1	SC5-SC5 (C01-C02)	0.240	constraint	
b_2	SC5-SN0 (C01-N04, C02-N05)	0.300	constraint	
b_3	SN0-SC5 (N04-C06, N05-C06)	0.250	constraint	
b_4	SC5-SC5 (C06-C07, C06-C08)	0.250	constraint	
b_5	SC5-SN0 (C07-N09, C08-N09)	0.310	10000	
		θ_0 (deg)	κ_θ (kJ mol ⁻¹)	
θ_1	VS-SC5-SN0 (V03-C06-N09)	138.00	250.00	
θ_2	SN0-SC5-SN0 (N04-C06-N05)	105.00	150.00	
θ_3	SN0-SN0-SN0 (N04-N05-N09, N05-N04-N09)	71.00	250.00	
		ϕ_0 (deg)	κ_ϕ (kJ mol ⁻¹ rad ⁻²)	
ϕ_1	SC5-SC5-SN0-SN0 (C01-C02-N05-N04)	1.00	50.00	
ϕ_2	SC5-SC5-SN0-SN0 (C02-C01-N04-N05)	1.00	50.00	
ϕ_3	SC5-SN0-SC5-SN0 (C02-N04-C06-N05)	-28.00	200.00	
ϕ_4	SC5-SN0-SC5-SN0 (C02-N09-C06-N05)	-45.00	200.00	
ϕ_5	SN0-SN0-SC5-SC5 (N04-N05-C07-C08)	2.69	14.12	2
		0.00	4.31	3
		0.08	2.31	4

dihedrals ϕ_1 and ϕ_2 are used to keep the dimethylbenzimidazole moiety plane, while ϕ_3 and ϕ_4 allow for the angle between the dimethylbenzimidazole backbone and phenyl substituent. ϕ_5 is needed to reproduce the dihedral profile around the dimethylbenzimidazole-phenyl connection, dihedral which has been fitted to reproduce the QM energy profile (see **Atomistic models** section). Bond and angle distributions are shown in Figure S8.

Chloroform. A model for chloroform (CLF) is available within the Martini force field. Based on the potential of mean force (PMF) computed for the dimerization of two PP molecules (see **PMF calculations** section), the C₆₀-CLF interactions were found to be too strong at the CG level. We note that CLF was not in the pool of solvents considered for the parametrization of the Martini C₆₀ model.^{S10} The C₆₀-CLF interactions have been thus reduced as explained in more detail in the **PMF calculations** section. The density of the CLF CG model is 1.45 g cm⁻³, in agreement with the experimental density (1.48 g cm⁻³).

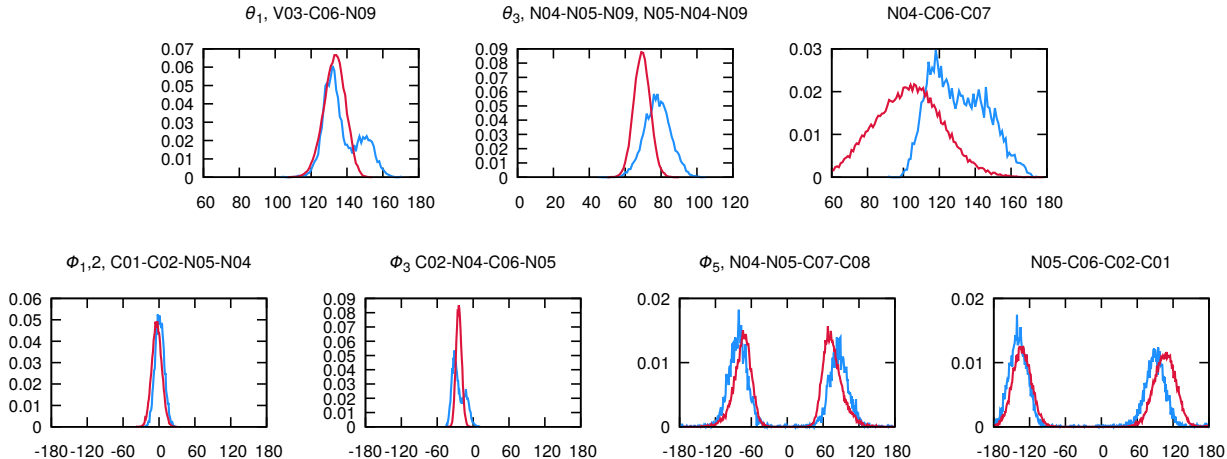


Figure S8: Bond and angle distributions for N-DMBI (Martini in red, GROMOS in blue). Each header indicates the degree of freedom whose distribution is shown (see Table S5).

Atomistic models. All-atom (AA) models have been used as a reference to parametrize the bonded parameters of the CG models and as reference for free energy profiles of dimerization (see PMF calculations section). They have been built based on the GROMOS 53A6 set of force field parameters.^{S11} The atomistic topologies were obtained as follows, following the procedure employed in Ref. S9: starting topologies obtained from the automated topology builder (ATB)^{S12,S13} were double-checked for consistency with the GROMOS 53A6 force field. Non-standard dihedral angles were checked by quantum mechanical calculations, as described below. HF/6-31G* charges computed with the dipole preserving analysis (DPA)^{S14} method as implemented in the GAMESS-UK code^{S15} are employed as partial charges on the atoms, if not stated otherwise.

PTEG-1. An AA model for PP has been obtained by merging the AA C₆₀ model developed by Monticelli,^{S10} which performs well both in terms of solid-state properties and partitioning between solvents,^{S10} to the phenylpyrrolidine fragment, whose parameters have been obtained following the general procedure outlined before. The TEG chain bonded parameters have been taken from the latest refinement of ether parameters within GROMOS 53A6 (the OXY+D extension^{S16,S17}). All the bonded parameters for the PTEG-1 AA model are listed in Table S6. The dihedral involving the rotation around the phenyl-pyrrolidine

Table S6: PTEG-1 atomistic bonded parameters. If the bonded parameters are standard GROMOS 53A6, the corresponding GROMOS label is shown in parentheses next to the bond (angle) equilibrium value and/or force constant.

Atoms	b_0 (nm)	κ_b (kJ mol ⁻¹ nm ⁻⁴)	
CF-CF (fullerene)	0.1450	$3.92 \cdot 10^5$	
CF-C	0.1529	$2.24 \cdot 10^5$	
	b_0 (nm)	κ_b (kJ mol ⁻¹ nm ⁻²)	
HC-C	0.1090 (gb_3)	$1.23 \cdot 10^7$ (gb_3)	
NT-C	0.1470 (gb_21)	$8.71 \cdot 10^6$ (gb_21)	
C-C (Py-Ph connection)	0.1520 (gb_26)	$5.43 \cdot 10^6$ (gb_26)	
C-C (phenyl)	0.1390 (gb_15)	$8.66 \cdot 10^6$ (gb_15)	
C-C (phenyl)	0.1390 (gb_15)	$8.66 \cdot 10^6$ (gb_15)	
C-C (ether)	0.1530 (gb_27)	$7.15 \cdot 10^6$ (gb_27)	
C-OE	0.1430 (gb_18)	$8.18 \cdot 10^6$ (gb_18)	
	θ_0 (deg)	κ_θ (kJ mol ⁻¹)	
CF-CF-CF (fullerene pentagons)	108.0	527.184	
CF-CF-CF (fullerene hexagons)	120.0	527.184	
CF-CF-C (fullerene - side chain)	112.50; 103.00	530.0 (ga_15); 465.00 (ga_7)	
CF-C-C (fullerene - side chain)	104.00	465.00 (ga_7)	
CF-C-C (fullerene - side chain)	109.50 (ga_11)	425.00 (ga_11)	
CF-C-C (fullerene - side chain)	111.00 (ga_15)	530.0 (ga_15)	
C-C-C	109.50 (ga_11)	425.00 (ga_11)	
C-NT-C	116.00 (ga_21)	620.00 (ga_21)	
C-NT-C (5-ring)	108.00 (ga_7)	465.00 (ga_7)	
NT-C-C (Py-Ph)	111.00 (ga_15)	530.00 (ga_15)	
HC-C-NT,C,OE,HC	109.50 (ga_11)	425.00 (ga_11)	
C-C-C (phenyl)	120.00 (ga_27)	530.00 (ga_27)	
C-C-CH (phenyl)	120.00 (ga_25)	505.00 (ga_25)	
OE-C-C, C-OE-C	111.00 (ga_15)	530.00 (ga_15)	
	ϕ_0 (deg)	κ_ϕ (kJ mol ⁻¹)	n
CF-CF-CF-CF	143.00	100.00	
C-C-C-C (phenyl)	0.00 (gi_1)	167.36 (gi_1)	
C-NT-C-CF	0.00 (gd_41)	3.77 (gd_41)	6
C-C-CF-CF	180.00 (gd_39)	1.00 (gd_39)	6
CF,HC-C,NT-C-C	180.00 (gd_39)	1.00 (gd_39)	6
CF-C-C-C (Py-Ph connection) ^a	180.00 (gd_39)	1.00 (gd_39)	6
C-OE-C-C; OE-C-C-OE	0.00; 0.00	0.931; 6.942	1
	0.00; 0.00	0.569; 3.312	2
	0.00; 0.00	4.682; 6.787	3
OE-C-C-HC	0.00 (gd_33)	5.4 (gd_33)	3

^a Checked at the B3LYP/6-31G* level of theory.

bond is a non-standard dihedral and has been therefore checked by electronic structure calculations. The potential energy surface as a function of the dihedral (highlighted in Figure S9b) has been computed at the B3LYP/6-31G* level of DFT, and it is plotted in Figure S9a (green dots). The same scan performed at the molecular mechanics level (Figure S9a, blue dots) shows excellent agreement for the two profiles, with discrepancies arising only at the maxima. However, being the barrier very high in both cases, the molecular conformations sampled will be confined around the two symmetric minima at 75° and -100° , making the dihedral correction unnecessary.

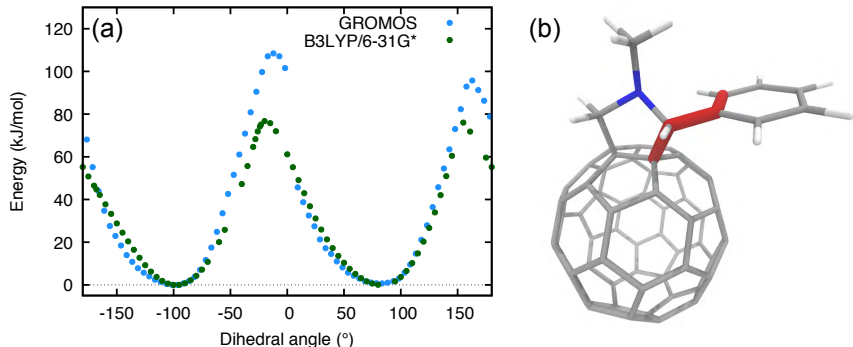


Figure S9: (a) DFT (B3LYP/6-31G*, green dots) *vs* GROMOS atomistic molecular mechanics (blue dots) energy profile for the (b) dihedral angle between the pyrrolidine and phenyl fragment of the sidechain of PP (highlighted in red).

Dopants. The torsion around the bond connecting the benzimidazole moiety to the phenyl one (dihedral angle highlighted in Figure S10b) has been also checked by electronic structure calculations. Compared to the DFT potential energy surface (Figure S10a, green dots), the initial GROMOS profile was unsatisfactory, presenting shallower minima and a lower torsion barrier. The difference between the DFT and initial GROMOS energy profiles was thus fitted to obtain parameters to refine the dihedral profile. The dihedral function used for the fit is a periodic type function implemented in GROMACS:

$$V_d(\phi_{ijkl}) = k_\phi(1 + \cos(n\phi - \phi_s)) \quad (\text{S1})$$

where the potential V_d of the dihedral ϕ between the ijk and jkl planes is given by a sum of

cosine terms with different multiplicity (n). The parameters which give rise to the fit shown in Figure S10 (blue dots) are reported in Table S7.

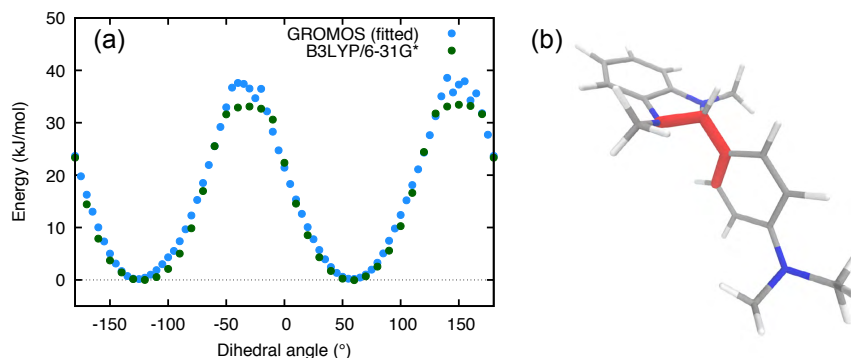


Figure S10: (a) DFT (B3LYP/6-31G*, green dots) *vs* modified (see text) GROMOS molecular mechanics (blue dots) energy profile for the (b) dihedral angle between the benzimidazole and phenyl moieties of N-DMBI (highlighted in red).

Chloroform. The standard CLF GROMOS 53A6 model has been used.^{S11} Note that charges are taken from Ref. S18, following Tironi and van Gunsteren.^{S19} The model gives a density of 1.56 g cm^{-3} , which is in reasonable agreement (+5%) with the experimental value of 1.48 g cm^{-3} .

GROMACS topology files of the CG and AA models used in the present work are available for download as part of the Supporting Information and on the Martini portal <http://cgmartini.nl>.

PMF calculations. Interactions between the molecules object of the study were validated by comparing dimerization potentials of mean force (PMFs) at the CG level with the corresponding AA ones. PMFs were calculated for the dimerization of two N-DMBI molecules, and two PP molecules, all in CLF solution. The calculations were performed through umbrella sampling as done in Ref. S9. Windows of at least 150 and 500 ns were carried out at the CG and AA levels, respectively, to ensure sufficient sampling. Figure S11 shows that CG PMFs are in line with atomistic ones. Attempts to further minimize the discrepancy between the atomistic and CG N-DMBI dimerization free energy profiles (by, for example, switching on non bonded interactions for the virtual site employed in the CG

Table S7: N-DMBI atomistic bonded parameters. If the bonded parameters are standard GROMOS 53A6, the corresponding GROMOS labelling is shown in parenthesis next to the bond (angle) equilibrium value and/or force constant.

Atoms	b_0 (nm)	κ_b (kJ mol ⁻¹ nm ⁻⁴)	
HC-C	0.1090 (gb_3)	$1.23 \cdot 10^7$ (gb_3)	
NT-C	0.1470 (gb_21)	$8.71 \cdot 10^6$ (gb_21)	
C-C (phenyl)	0.1390 (gb_15)	$8.66 \cdot 10^6$ (gb_15)	
C-C (Py-Ph connection)	0.1520 (gb_26)	$5.43 \cdot 10^6$ (gb_26)	
	θ_0 (deg)	κ_θ (kJ mol ⁻¹)	
HC,C-C-C,NT,HC	109.50 (ga_11)	425.00 (ga_11)	
C-C-C (phenyl)	120.00 (ga_27)	530.00 (ga_27)	
C-C-CH (phenyl)	120.00 (ga_25)	505.00 (ga_25)	
C-NT-C (5-ring)	108.00 (ga_7); 107.00; 101.00	465.00 (ga_7)	
C-(5-ring)	120.00	620.00 (ga_21)	
C-C-NT (rings connection)	126.00 (ga_37)	640.00 (ga_37)	
	ϕ_0 (deg)	κ_ϕ (kJ mol ⁻¹)	n
C-C-C-C (phenyl)	0.00 (gi_1)	167.36 (gi_1)	
HC,NT-C-C,NT-C	180.00 (gd_39)	1.00 (gd_39)	6
C-NT-C-NT	0.00 (gd_41)	3.77 (gd_41)	6
C-C-C-C,HC (phenyl)	180.00	41.80	2
C-C-NT-C	180.00	33.50	2
NT-C-C-C ^a	-63.89	6.55	2
	52.49	0.92	4
	-5.65	1.32	6

^a fitted to QM data.

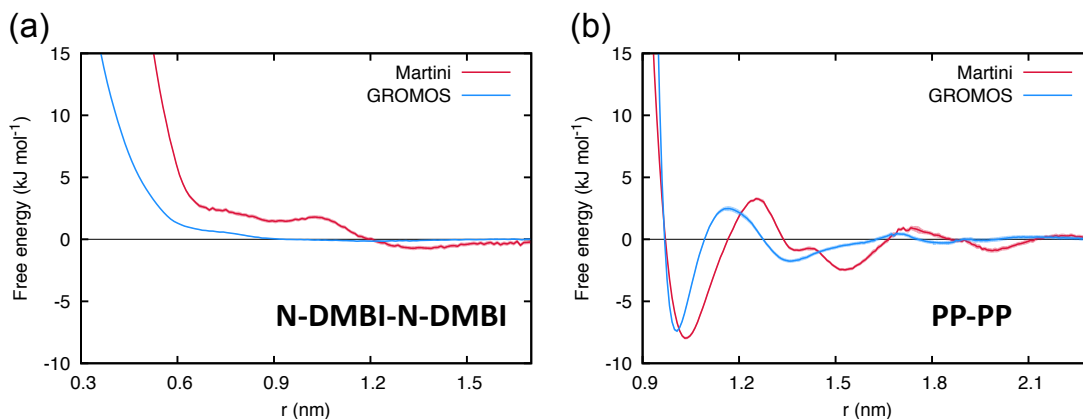


Figure S11: PMFs of dimerization for the (a) dopant-dopant, and (b) PP-PP pairs in CLF. GROMOS PMFs are in blue, while Martini in red.

N-DMBI model) resulted in the appearance of a minimum located at around 0.7 nm. Given the clear absence of such minimum on the atomistic free energy surface, the final parameters were chosen to be the ones which give rise to the profile shown in Figure S11a. In the case of PP, the interaction between the CNP (which describes the C₆₀ fullerene) and the C4 (representing CLF) particles had to be scaled down from 3.5 kJ mol⁻¹ to 3.15 kJ mol⁻¹. This leads to a PMF of dimerization in CLF in good agreement with the atomistic one. As noted earlier, CLF was not in the pool of solvents considered for the parametrization of the Martini C₆₀ model.^{S10}

3.2.2 Analysis details

Number of Contacts. Number of contacts are computed employing the `gmx mindist` GROMACS tool with a cutoff distance of 0.6 nm, a length which comprises the nearest neighbour CG sites around a CG particle. More details are given in Ref. S9. In this case, for the dopant molecules, side chain beads are excluded from the counting (the N09 bead in the case of N-DMBI, and the four SP0 beads in the case of TEG-DMBI).

A planar heterojunction and a completely (randomly) intermixed morphologies have been used as the two opposite reference (extreme) cases of mixing to normalize the number of computed DMBI–PTEG-1 contacts. These two configurations have been generated using a starting configuration obtained with the software `packmol`^{S20} which has been then equilibrated in NPT conditions.

4 NMR spectra

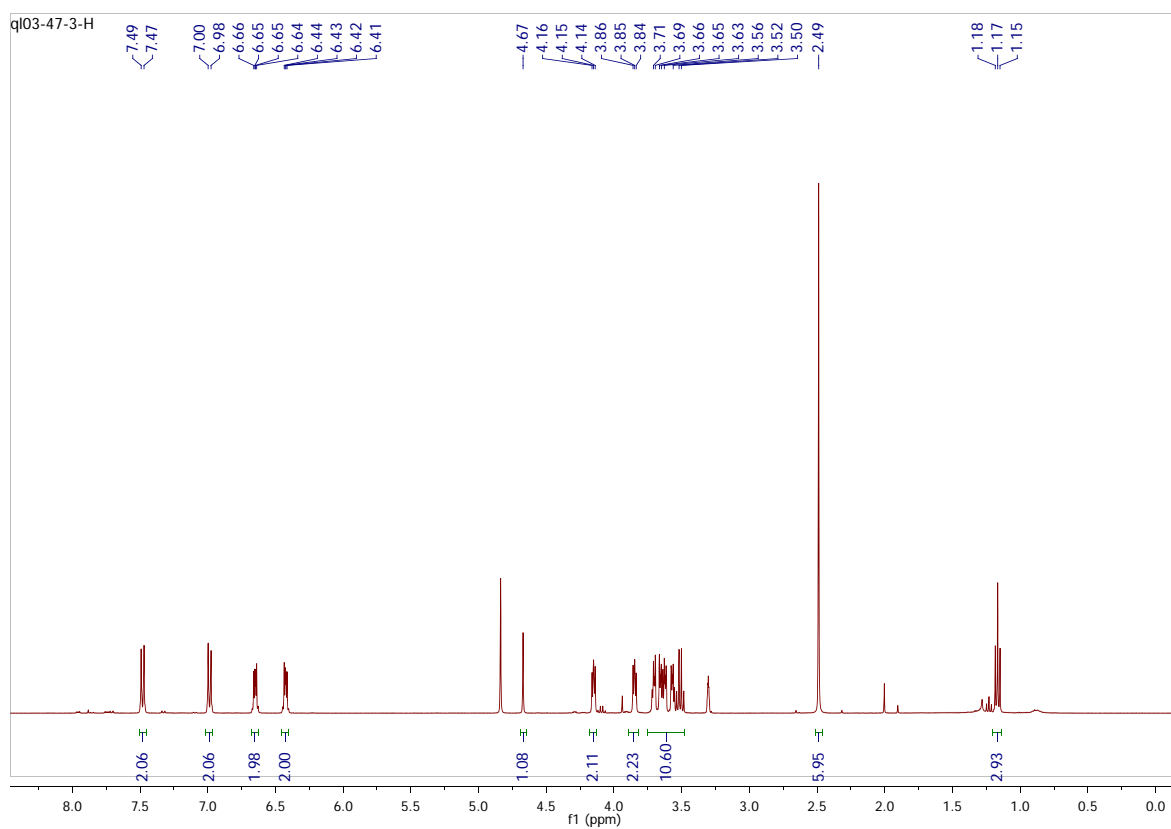


Figure S12: ^1H NMR spectrum of TEG-DMBI

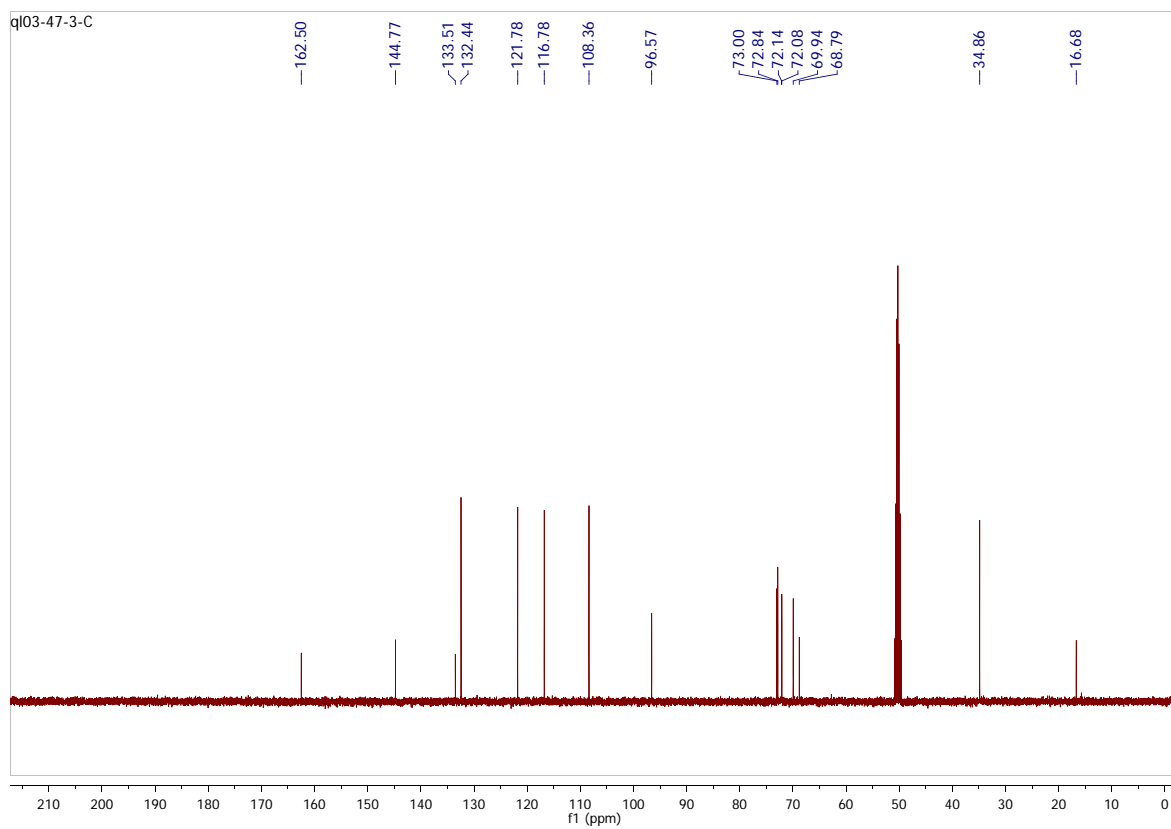


Figure S13: ^{13}C NMR spectrum of TEG-DMBI

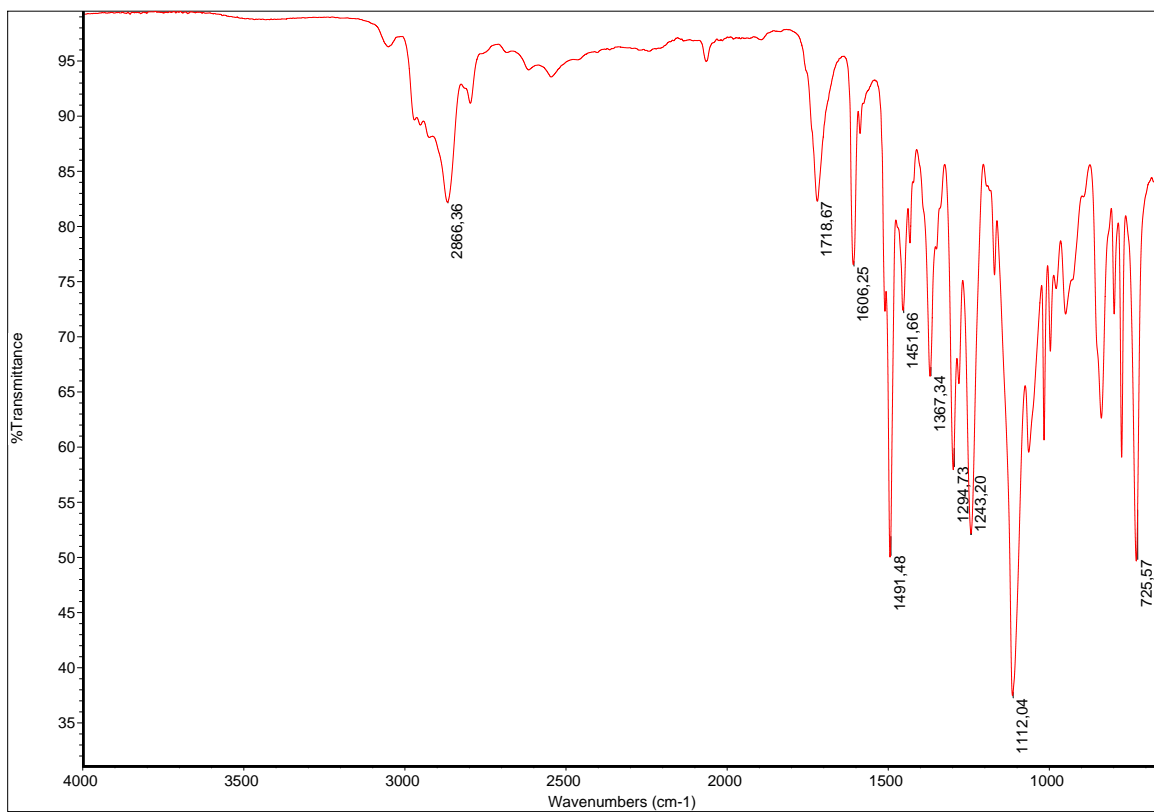


Figure S14: IR spectrum of TEG-DMBI

References

- (S1) Zhu, X.-Q.; Zhang, M.-T.; Yu, A.; Wang, C.-H.; Cheng, J.-P. Hydride, hydrogen atom, proton, and electron transfer driving forces of various five-membered heterocyclic organic hydrides and their reaction intermediates in acetonitrile. *Journal of the American Chemical Society* **2008**, *130*, 2501–2516.
- (S2) Pasveer, W.; Cottaar, J.; Tanase, C.; Coehoorn, R.; Bobbert, P.; Blom, P.; De Leeuw, D.; Michels, M. Unified description of charge-carrier mobilities in disordered semiconducting polymers. *Physical review letters* **2005**, *94*, 206601.
- (S3) Liu, J.; Qiu, L.; Portale, G.; Koopmans, M.; ten Brink, G.; Hummelen, J. C.; Koster, L. J. A. N-Type Organic Thermoelectrics: Improved Power Factor by Tailoring HostDopant Miscibility. *Advanced Materials* **2017**, DOI: 10.1002/adma.201701641, 1701641.
- (S4) Wei, P.; Oh, J. H.; Dong, G.; Bao, Z. Use of a 1 H-benzoimidazole derivative as an n-type dopant and to enable air-stable solution-processed n-channel organic thin-film transistors. *Journal of the American Chemical Society* **2010**, *132*, 8852–8853.
- (S5) Marrink, S. J.; Risselada, H. J.; Yefimov, S.; Tieleman, D. P.; de Vries, A. H. The MARTINI Force Field: Coarse Grained Model for Biomolecular Simulations. *The Journal of Physical Chemistry B* **2007**, *111*, 7812–7824.
- (S6) Lee, H.; de Vries, A. H.; Marrink, S. J.; Pastor, R. W. A Coarse-Grained Model for Polyethylene Oxide and Polyethylene Glycol: Conformation and Hydrodynamics. *The Journal of Physical Chemistry B* **2009**, *113*, 13186–13194.
- (S7) Rossi, G.; Fuchs, P. F. J.; Barnoud, J.; Monticelli, L. A Coarse-Grained MARTINI Model of Polyethylene glycol and of Polyoxyethylene Alkyl Ether Surfactants. *The Journal of Physical Chemistry B* **2012**, *116*, 14353–14362.

- (S8) Bulacu, M.; Goga, N.; Zhao, W.; Rossi, G.; Monticelli, L.; Periolo, X.; Tieleman, D. P.; Marrink, S. J. Improved Angle Potentials for Coarse-Grained Molecular Dynamics Simulations. *Journal of Chemical Theory and Computation* **2013**, *9*, 3282–3292.
- (S9) Alessandri, R.; Uusitalo, J. J.; de Vries, A. H.; Havenith, R. W. A.; Marrink, S. J. Bulk Heterojunction Morphologies with Atomistic Resolution from Coarse-Grain Solvent Evaporation Simulations. *Journal of the American Chemical Society* **2017**, *139*, 3697–3705.
- (S10) Monticelli, L. On Atomistic and Coarse-Grained Models for C₆₀ Fullerene. *Journal of Chemical Theory and Computation* **2012**, *8*, 1370–1378.
- (S11) Oostenbrink, C.; Villa, A.; Mark, A. E.; van Gunsteren, W. F. A Biomolecular Force Field Based on the Free Enthalpy of Hydration and Solvation: The GROMOS Force-Field Parameter Sets 53A5 and 53A6. *Journal of Computational Chemistry* **2004**, *25*, 1656–1676.
- (S12) Malde, A. K.; Zuo, L.; Breeze, M.; Stroet, M.; Poger, D.; Nair, P. C.; Oostenbrink, C.; Mark, A. E. An Automated Force Field Topology Builder (ATB) and Repository: Version 1.0. *Journal of Chemical Theory and Computation* **2011**, *7*, 4026–4037.
- (S13) Koziara, K. B.; Stroet, M.; Malde, A. K.; Mark, A. E. Testing and validation of the Automated Topology Builder (ATB) version 2.0: prediction of hydration free enthalpies. *Journal of Computer-Aided Molecular Design* **2014**, *28*, 221–233.
- (S14) Thole, B. T.; van Duijnen, P. T. A General Population Analysis Preserving the Dipole Moment. *Theoretica chimica acta* **1983**, *63*, 209–221.
- (S15) Guest, M. F.; Bush, I. J.; van Dam, H. J. J.; Sherwood, P.; Thomas, J. M. H.; van Lenthe, J. H.; Havenith, R. W. A.; Kendrick, J. The GAMESS-UK Electronic Structure Package: Algorithms, Developments and Applications. *Mol. Phys.* **2005**, *103*, 719–747.

- (S16) Horta, B. A.; Fuchs, P. F.; van Gunsteren, W. F.; Hunenberger, P. H. New interaction parameters for oxygen compounds in the GROMOS force field: Improved pure-liquid and solvation properties for alcohols, ethers, aldehydes, ketones, carboxylic acids, and esters. *Journal of Chemical Theory and Computation* **2011**, *7*, 1016–1031.
- (S17) Fuchs, P. F.; Hansen, H. S.; Hunenberger, P. H.; Horta, B. A. A GROMOS parameter set for vicinal diether functions: properties of polyethyleneoxide and polyethyleneglycol. *Journal of Chemical Theory and Computation* **2012**, *8*, 3943–3963.
- (S18) Dietz, W.; Heinzinger, K. Structure of liquid chloroform. A comparison between computer simulation and neutron scattering results. *Berichte der Bunsengesellschaft für physikalische Chemie* **1984**, *88*, 543–546.
- (S19) Tironi, I. G.; van Gunsteren, W. F. A Molecular Dynamics Simulation Study of chloroForm. *Molecular Physics* **1994**, *83*, 381–403.
- (S20) Martínez, L.; Andrade, R.; Birgin, E. G.; Martínez, J. M. PACKMOL: a Package for Building Initial Configurations for Molecular Dynamics Simulations. *Journal of computational chemistry* **2009**, *30*, 2157–2164.